

Bottom-Up Approach to Assess the Molecular Structure of Aqueous Poly(*N*-Isopropylacrylamide) at Room Temperature via Infrared Spectroscopy

Habtom B. Gobeze, Jianbo Ma, Fedra M. Leonik, and Daniel G. Kuroda*

Cite This: *J. Phys. Chem. B* 2020, 124, 11699–11710

Read Online

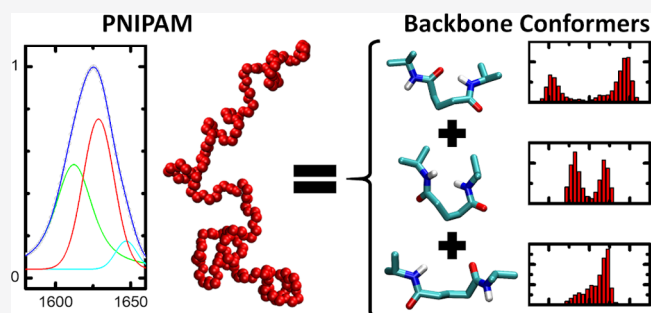
ACCESS |

Metrics & More

Article Recommendations

Supporting Information

ABSTRACT: The structure of poly(*N*-isopropylacrylamide) (PNIPAM) in solution is still an unresolved topic. Here, the PNIPAM structure in water was investigated using a bottom-up approach, involving the monomer, dimer, and trimer, and a combination of infrared (IR) spectroscopies as well as molecular dynamics simulations. The experiments show that the monomer and oligomers exhibit a broad and asymmetric amide I band with two underlying transitions, while PNIPAM presents the same major transitions and a minor one. Analysis of the 2D IR spectra and theoretical modeling of the amide I band indicates that the two transitions of the monomer do not have the same molecular origin as the oligomers and the polymer. In the monomer, the two bands originate from the ultrafast rotation of its ethyl group, which leads to different solvation structures for the various rotational conformers. In the case of the oligomers, the asymmetry and splitting of the amide I band is caused by the vibrational coupling among adjacent amide side chains. Moreover, it is deduced from the simulations that the oligomers have three distinct backbone conformations for neighboring amides. In particular, two of the backbone conformations have a closed and compact structure, while in the third, the backbone is open and elongated. The bottom-up approach allowed us to infer that such backbone conformations exist in PNIPAM as well. Consequently, the two major amide I transitions of the polymer are also assigned to split amide I transitions resulting from the vibrationally coupled nearest-neighboring amides. In contrast, the additional minor transition observed in PNIPAM is assigned to unsolvated amide units of the polymer. The proposed molecular model successfully describes that PNIPAM amide I band changes with temperature in terms of its molecular structure. This new model strongly suggests that PNIPAM does not have a completely random backbone structure, but has distinct backbone conformers between neighboring amides.



INTRODUCTION

Thermoresponsive polymers are stimuli-responsive or “smart” polymers that show phase transition in response to a change in temperature.¹ Water-soluble thermoresponsive polymers have been widely studied because of their unique features and potential applications in medicine and biomaterials.^{2–10} Poly(*N*-isopropylacrylamide) (PNIPAM) has been one of the most extensively studied archetypal water-soluble thermoresponsive polymer.¹¹ PNIPAM shows a reversible phase transition in water with a lowest critical solution temperature (LCST) of ~32 °C. Since the first report by Heskins and Guillet in 1968,¹² PNIPAM has attracted immense attention as a smart material with a wide range of possible uses, such as textile,¹³ biomaterials,¹⁴ drug delivery,¹⁵ chromatography,¹⁶ and biomedical applications because of its near physiological LCST.¹⁷

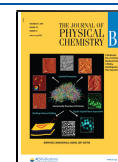
In the past few decades, the molecular mechanism of PNIPAM thermal phase separation in aqueous solutions was extensively investigated.^{18–27} For this purpose, different

experimental techniques, including but not limited to turbidimetry,²⁸ calorimetry,^{29–32} fluorescence,^{33,34} light scattering,^{20–24,35,36} Raman spectroscopy,^{18,19} nuclear magnetic resonance,^{37,38} and infrared (IR) spectroscopy,^{25,26,28,39–46} have been used. However, the mechanism of the PNIPAM phase transition has been principally derived from dynamic and static light scattering experiments, where it has been indisputably established that the dimensionality of the polymer chain abruptly changes at the LCST.^{20–24,35,36} This result leads to the current and most accepted mechanism of phase transition of PNIPAM involving a change in the polymer

Received: September 16, 2020

Revised: November 25, 2020

Published: December 11, 2020



conformation from a swollen and well-solvated random coil to tightly packed globular chain occurring at the LCST.

The details of the molecular mechanism behind the hydrophobic collapse of PNIPAM at the LCST have been investigated by a variety of techniques, including light scattering, Raman spectroscopy, and Fourier transform infrared spectroscopy (FTIR).^{22,25,27} The first FTIR reports concluded that the polymer undergoes a dehydration of the isopropyl groups during the LCST.²⁵ In addition, it was noted that an underlying peak grows within the amide I band above the LCST. This "extra" peak was assigned to the formation of an intramolecular hydrogen bond between the C=O and the N-H groups of different amide side chains. From these IR spectroscopy studies, it was proposed that the driving force behind the coil-to-globule transition was the dehydration of the polymer chains, which induces hydrophobic interactions between the isopropyl groups and ultimately drives the collapse of the PNIPAM chain. However, more recent PNIPAM experimental studies did not find intra- or interamide hydrogen bond to be a cause for the collapse.^{27,47} Rather, the studies proposed that the amide bonds of PNIPAM were not involved in interamide hydrogen bonding in the collapsed state. Hence, it has been lately inferred that the PNIPAM mechanism of the hydrophobic collapse was because of a difference in the hydration of the polymer below and above the LCST. Moreover, another study showed that the polymer contains ~66% water even in its collapsed state, which reinforced the idea that the amide is not fully dehydrated during the polymer phase transition.²⁰ A more recent work has proposed that the hydration of the PNIPAM backbone also plays a major role in the hydrophobic collapse of PNIPAM during its phase transition.⁴⁸

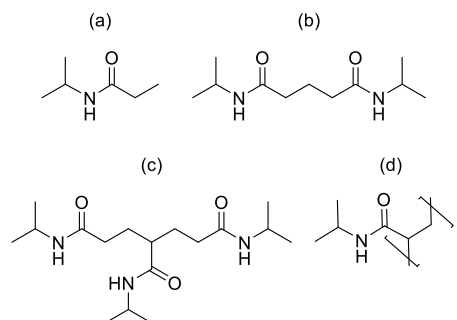
The hydration of PNIPAM and its oligomers across the LCST has been investigated mainly via high-frequency dielectric relaxation techniques.^{49,50} Overall, these studies observed a significant decrease in the number of hydration shell water molecules around the PNIPAM globule state when the temperature was close to the LCST, but they also noted that the dehydration was only partial. The role of water solvation dynamics and intramolecular hydrogen bonding in the hydrophobic collapse of aqueous PNIPAM has been reinforced by computational studies, which showed via molecular dynamics (MD) simulations that the structure of the water molecules around the polymer is different below and above the LCST.^{51,52} Moreover, the studies revealed that two possible polymer conformations exist in the collapsed state: one with stable intrachain hydrogen bonding (tightly collapsed) and the other with less stable hydrogen bonding (loosely collapsed).⁵² While the phase transition mechanism provides an insight into the molecular changes during the phase transition, the contribution of PNIPAM structural conformations to the phase transition mechanism is yet to be found.

The PNIPAM backbone conformation has been studied by both experimental and computational methods. While it has been observed experimentally that the coil and globule conformations are thermodynamically stable below and above the LCST, respectively, it has also been determined that other intermediate conformers of the polymer exist.²⁰ A computational study investigating single chains demonstrated that the conformational changes of the oligomers (bending of the backbone) occurred as temperature increased because of the destabilization of the hydration shell of the hydrophobic

groups.⁵³ Recently, an atomistic study on an ensemble of PNIPAM chains using biased and unbiased MD simulations revealed that the random-coil conformation is thermodynamically more stable than the globule conformation at temperature below the LCST by 21 kJ/mol, while the situation is reverse above the LCST, where the globule conformation is thermodynamically favored by 21 kJ/mol.⁵⁴ Interestingly, the study also revealed that the random-coil and the globule conformations contain a large ensemble of conformations, which do not correspond to a well-defined structure in the polymer. However, the existence of different PNIPAM backbone conformations is yet to be experimentally demonstrated.

Here, the solvation and conformational structure of PNIPAM solutions are studied using steady-state and time-resolved IR spectroscopies, where the amide I modes of the polymer acts as a reporter. In particular, the amide I mode has been shown to be sensitive to structural changes resulting from the strong vibrational coupling among amides.^{55–58} Hence, amides have been extensively used to study the structure of polypeptides, biomolecules, and secondary structures of proteins.^{59–64} In addition, it is well known that the amide I vibrational mode is a good reporter of the molecular environment.^{65–69} Thus, this study is focused on characterizing the molecular environment and structure of PNIPAM and its oligomers using the amide I transition of the isopropyl amide units. To this end, PNIPAM and oligomers with one (monomer), two (dimer), and three (trimer) isopropyl amide units (Scheme 1) were synthesized and investigated in D₂O

Scheme 1. Chemical Structure of Monomer (a), Dimer (b), Trimer (c), and PNIPAM (d)



using FTIR, two-dimensional IR spectroscopy (2D IR). Infrared spectroscopies are ideal tools for studying the molecular structure and dynamics of the oligomers and PNIPAM because both techniques provide amide bond specific information. Particularly, 2D IR spectroscopy can provide sub picosecond dynamical information of the molecular arrangements and hydration dynamics of the amide units of the polymer.^{59,60,70,71} Furthermore, the observation and characterization of structural constraints via excitonic coupling in systems undergoing ultrafast conformational changes are an unrivaled use of 2D IR spectroscopy in solution and undergoing conformational changes.^{72–74} Finally, MD simulations complemented our studies by providing a molecular picture of the process giving rise to the observed ultrafast dynamics.

METHODS

Materials and Sample Preparation. Poly(*N*-isopropylacrylamide) (PNIPAM) (Polyscience Inc., $M_n = 40,000$ g/mol) was dried at 85 °C under a vacuum before use. Deuterium oxide (99.9% D) was purchased from Acros Organics and used as received. Tetrahydrofuran (THF) was purchased from Sigma-Aldrich and was purified of water contamination by passing through an alumina column under argon. Monomer, dimer, and trimer were synthesized following procedures detailed in the [Supporting Information](#). All solutions were passed through a 0.2 μm filter before measurements to remove any possible undissolved solids. The concentrations used are 10 mM for monomer in THF and D₂O, 40 mM for dimer in D₂O and THF, 40 mM for trimer in D₂O, and 40 mM and 0.5mM for PNIPAM in THF and D₂O, respectively.

Linear Infrared Spectroscopy. Linear IR measurements were performed using a Bruker Tensor 27 with a liquid nitrogen-cooled narrow band MCT detector. All samples were measured with 0.5 cm^{-1} resolution and averaged from 40 scans. The solution samples were held in an O-ring sealed sample cell with two CaF₂ windows separated by a Teflon spacer having different thickness depending on concentration. For THF experiments, sample cells were prepared in a nitrogen-filled glovebox to minimize exposure to moisture. In the temperature-dependent IR studies, the temperature of the sample cell was controlled by placing it in a Harrick cell holder connected to a commercial chiller.

Two-Dimensional Infrared Spectroscopy. The setup used for 2D IR experiments has been previously detailed in the literature, so only a short description is provided here.⁷⁵ The input IR pulses were generated by a Spectra Physics Spitfire Ace Ti/sapphire amplifier at a repetition rate of 5 kHz, in combination with an OPA-800C and a difference frequency generation crystal. These input IR pulses were then split into three replicas and later focused on the sample using the well-known boxcar geometry.⁷⁰ The time intervals τ (time between the first pulse and the second pulse), T_w (time between the second and the third pulse), and t (time between the third pulse and the photon echo) were monitored by computer-controlled four translational stages (PI miCos). The generated photon echo with pulses in parallel polarization ($\langle\text{XXXX}\rangle$) in the phase-matching direction ($-\mathbf{k}_1 + \mathbf{k}_2 + \mathbf{k}_3$) was heterodyned with a fourth pulse (local oscillator) and later dispersed by a Triax Monochromator. The resulting nonlinear signal and local oscillator were detected with a liquid nitrogen-cooled 64 element MCT array detector (Infrared Systems Developments). Here, 2D IR data were collected by scanning τ time from -3.5 to $+3.5$ ps in increments of 5 fs for each waiting time in order to collect both the rephasing and non-rephasing data by switching the time ordering.⁷⁰ Signals were collected for waiting times from 0 to 3.0 ps in steps of 0.25 ps. In all the measurements, the local oscillator always preceded the photon echo signal by ~ 0.5 ps. The time domain signal, collected as a function of (τ, T, λ_t) via a monochromator-array detection, is transformed into the 2D IR spectra $(\omega_\nu, T, \omega_t)$ by means of Fourier transforms. A detailed explanation of the Fourier analysis has been described elsewhere.⁷⁶

MD Simulations. Classical MD simulations with periodic boundary conditions were performed by the Large-scale Atomic/Molecular Massively Parallel Simulator (LAMMPS).⁷⁷ For each of the oligomers (monomer, dimer, and trimer), a box size of 25 Å \times 25 Å \times 25 Å built by Packmol⁷⁸ with one

oligomer chain and 500 water molecules was used. To study the aggregation or intermolecular interaction, two oligomer chains and 500 water molecules were placed in the box. The oligomers and the water molecules were described using the Optimized Potentials for Liquid Simulations (OPLSAA) force field and the extended simple point charge (SPC/E) model, respectively.^{54,79,80} Note that these two force fields have been shown to reproduce the experimental properties of PNIPAM in aqueous solutions.^{54,79,80} The systems were first equilibrated in the NVT ensemble for 1 ns followed by a 10 ns isothermal-isobaric production run (in the NPT ensemble) with time steps of 1 fs. In all cases, the simulation temperature was 300 K, except for the dimer at both 300 and 350 K, and a Nose–Hoover thermostat with a damping constant of 1 ps was used. For analysis of the dihedral angle in evaluating the rotational conformations of the monomer and the dimer, MD trajectories from a simulation conducted under the same conditions but with production run of 1 ns and damping constant of 50 fs are used. The time step in all the simulations was 1 fs. The long-range electrostatics was accounted for using the Ewald method.⁸¹

RESULTS

The FTIR spectra of the monomer, dimer, trimer and PNIPAM ([Scheme 1](#)) in D₂O were first investigated. The linear IR spectra of these solutions in the amide I region at room temperature are shown in [Figure 1](#). All the samples show

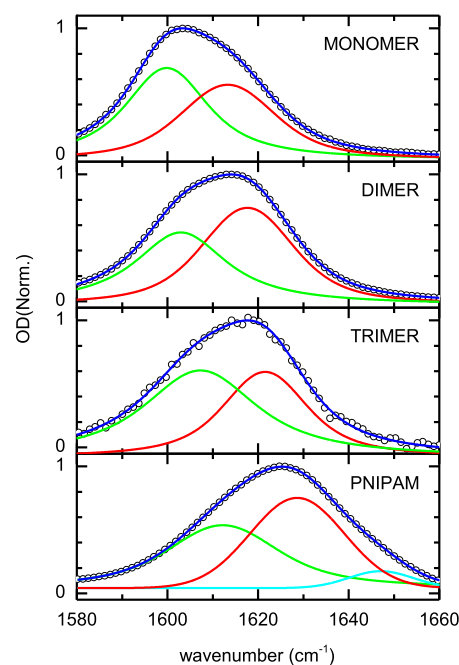


Figure 1. Linear IR spectra of the amide I band of the monomer, dimer, trimer, and PNIPAM in D₂O at room temperature. The background-subtracted experimental data (circles) and the Voigt fits are represented by circles and lines (blue, green, and red), respectively.

a broad and asymmetric band corresponding to the amide I transition. The monomer has an amide I band located at 1603 cm^{-1} with an fwhm of 29.33 cm^{-1} , while the dimer and the trimer are blueshifted by 11 and 14 cm^{-1} and have an fwhm of 33.60 and 33.36 cm^{-1} , respectively. Similarly, the amide I of PNIPAM is a broad and asymmetric band (fwhm ~ 37.83

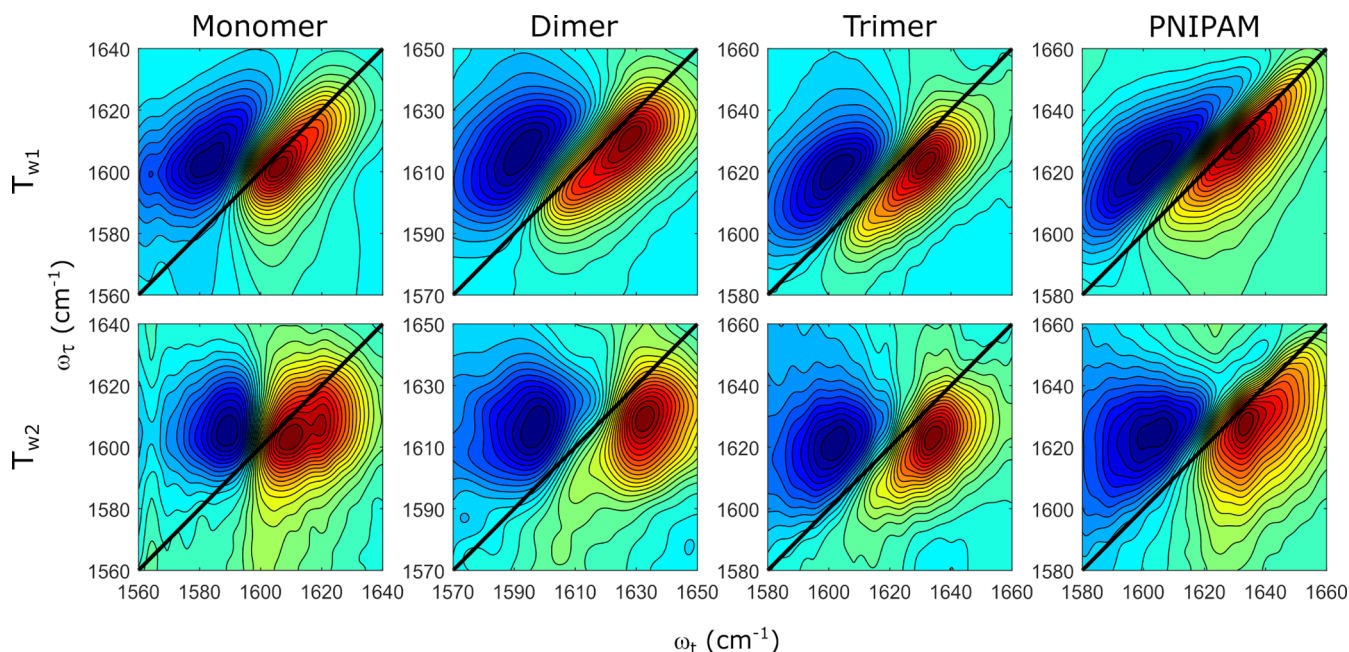


Figure 2. 2D IR spectra of the monomer, dimer, trimer, and PNIPAM in D₂O. The waiting time T_{w1} is 0 fs for all samples and T_{w2} is 3.0 ps for all except for the trimer, which is 1.5 ps.

cm⁻¹) and is centered at 1625 cm⁻¹. Compared to the monomer, the amide I band in PNIPAM is blueshifted by ~22 cm⁻¹. Overall, an increasing blue shift in the amide I frequency is observed as the number of polymer units increases.

The linear IR studies were extended to 2D IR spectroscopy. The 2D IR spectra of the monomer, dimer, trimer, and PNIPAM in the amide I region are shown in Figure 2. In all the investigated solutions, the 2D IR spectra show a positive peak (red) positioned along the diagonal line (black line corresponding to $\omega_\tau = \omega_t$), which is because of vibrational transitions involving the ground state ($\nu = 0$) and the first excited state ($\nu = 1$), that is, ground state bleach and stimulated emission. The other diagonal negative peak (blue) appearing at lower probe frequencies (ω_t) correspond to vibrational transition from the first excited state ($\nu = 1$) to the second excited state ($\nu = 2$) because of excited state absorption. This negative peak appears at lower probe frequency as a consequence of the anharmonic vibrational potential.

The 2D IR spectra show that all the samples have elongated and tilted peaks along the diagonal at $T_w = 0$ fs from homogeneous and inhomogeneous broadening of the vibrational transition.⁷⁰ The peak shapes also present a temporal evolution as seen by their change into more upright and round (symmetrical) peaks at later waiting times (Figure 2). The changes in the peak shapes evidence the process of spectral diffusion.⁷⁰ In addition, at longer waiting times, some of the samples display cross peaks in their 2D IR spectra. These cross peaks could be indicative of a chemical exchange and/or vibrational energy transfer because of vibrational coupling. These cross peaks are clear in the monomer and polymer 2D IR spectra, but they are not clearly visible in the other two samples.

DISCUSSION

The broad and asymmetric amide I bands of the monomer, oligomers, and PNIPAM in D₂O (Figure 1) evidence the

presence of more than one amide I transition within the main band. However, because of the different processes giving rise to the observed IR spectra, each of the samples is discussed separately in the following sections.

Monomer. The broad and asymmetric amide I band of the monomer in D₂O (Figure 1) evidences the presence of more than one transition within the amide I band. This amide band is well modeled with two Voigt profiles (Figure 1) and agrees with the temperature-dependent IR spectra, which shows the existence of two components (not shown). In addition, the enthalpy change (ΔH^0) observed in the van't Hoff plot derived from the temperature dependence study was found to be 1.1 ± 0.1 kcal/mol (see Supporting Information).⁸² While the two peaks could account for amide solvation shell with different numbers of hydrogen bonds, the enthalpy change is too small to account for the change in the amide-D₂O interaction because it has been previously shown that this interaction is -4.3 to -7.2 kcal·mol⁻¹ for a structurally similar amide molecule [*N*-methylacetamide, (NMA)].^{83,84} Moreover, the observed cross peaks have not been previously seen in NMA suggesting that the mechanism based exclusively on hydrogen bond exchange cannot explain the observed off-diagonal features. Another possible reason is that the bands arise from two solvation structures associated with relatively stable rotational conformers. It is well known that rotation-induced ultrafast transient changes in geometry such as isomerization and fluxional rearrangement in small organic molecules and organometallic complexes have a low energy barrier, which is in the range of 2–3 kcal/mol.^{73,85,86} This hypothesis is supported by conformation analysis of the side chain from the MD simulation. Analysis of the dihedral angle between the two carbons of the ethyl group and the carbonyl bond of the amide reveals not only that the ethyl group wiggles between -62 and $+62^\circ$ but also that its dynamics is in the picosecond time scale (τ) = 0.5 ps (see Supporting Information). This hypothesis is further supported by the 2D IR spectra of the monomer which

exhibits a clear cross-peak growth between the two bands at $T_w = 3.0$ ps (Figure 2). Note that other mechanisms such as amide cis and trans isomerization and aggregation are discarded because the spectra of the monomer in THF (see Supporting Information) as well as a concentration dependence study in D_2O (not shown) do not show the spectral signatures consistent with either of these two hypothesis. In addition, the presence of a single amide I band for the monomer in THF (see Supporting Information) reinforces the idea of observing conformers in the D_2O IR spectrum. In THF, the different sidechain conformers are expected to coexist and affect the solvation shell formed. However, the different THF solvation shells corresponding to the sidechain conformers do not produce changes in the amide I frequency of the monomer because THF lacks any strong and directional interaction with the amide. In water, the rotation of the monomer sidechain also causes changes in the arrangement (directionality and geometry) of water molecules directly hydrating the amide. Nonetheless, these different hydration shells are likely to result in different amide I frequencies because the directionality of the hydrogen bond between water molecules and the amide has a strong impact in the amide I mode.⁸⁷

The molecular picture of the different monomer conformers being fully solvated by water molecules is consistent with the spectral diffusion rate derived from the 2D IR spectra.⁷⁰ Here, the spectral diffusion, retrieved using the slope methodology within ± 5 cm^{-1} of the 2DIR peak maximum,⁸⁸ shows a decay

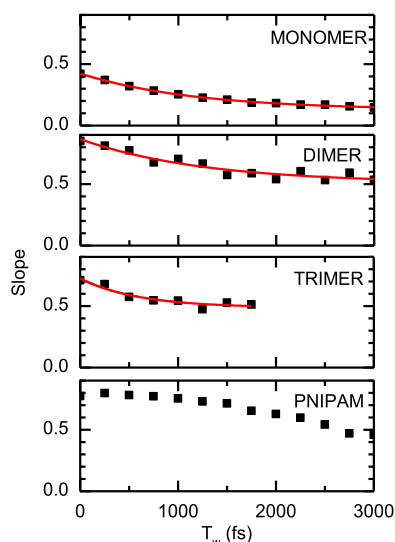


Figure 3. Slope as a function of waiting time for monomer, dimer, trimer, and PNIPAM. Lines represent the models as described in the text. Note that the trimer slope could not be properly analyzed after 1.5 ps because of the low solubility of the sample and the presence of the grating signal of water.⁹²

trend as a function of waiting time (Figure 3), which is well modeled with a function of the form

$$y = A \cdot e^{(-T_w/\tau)} + y_0 \quad (1)$$

where A is the amplitude, τ is the decay time, T_w is the waiting time, and y_0 is the offset. The decay time is found to be 1.2 ± 0.1 ps (Table 1) and agrees well with the spectral diffusion rate previously reported for NMA in D_2O , which has been shown to be fully hydrated.⁸⁹ Moreover, the slope exhibits the

Table 1. Exponential Fitting Parameters of the Slope Data as Described in the Text

sample	τ (ps)	y_0	A
monomer	1.2 ± 0.1	0.13 ± 0.01	0.30 ± 0.01
dimer	1.3 ± 0.4	0.51 ± 0.04	0.36 ± 0.04
trimer	0.6 ± 0.2	0.49 ± 0.03	0.24 ± 0.04

presence of an offset (y_0) in agreement with the presence of the monomer conformers with slightly different frequencies within the main amide I band as seen by the presence of the cross-peak.⁹⁰ Overall, the result indicates that the different monomer conformers perceive a similar hydrogen bonding environment of water, but the difference in frequency between the amide I bands associated with the conformers showcases a discrepancy in their solvation shells arising from either different number of hydrogen bonds or different arrangement of water molecules as a consequence of the side chain rotation.^{86,91} The mechanism of chemical exchange in the monomer is beyond the scope of this paper and will be addressed in a future study.

Dimer. Similar to the monomer, the dimer presents an asymmetric amide I band, which is well modeled with two Voigt profiles centered at 1603 and 1617 cm^{-1} (see Supporting Information). These bands are blueshifted from the monomer by 3 and 4 cm^{-1} , respectively. The 2D IR spectra agree with the presence of two underlying bands from the linear IR, but at slightly different positions: 1608 and 1620 cm^{-1} . The aqueous solution of the dimer does not present an easily identifiable cross-peak in the 2D IR spectra within the experimental waiting time of $T_w = 3.0$ ps even though the asymmetry of the amide I band in FTIR spectra and the difference spectra from temperature dependence (not shown) evidence the presence of two bands. Unlike in the monomer, the bulkiness of the sidechain in the dimer should slow down the thermally induced rotation of this group. This is consistent with the analysis of the dynamics of the dihedral angle between the carbonyl bond and the nearest C–C bond of the backbone chain from the MD simulation, which shows a slowdown of 12 times when compared to the monomer ($\langle \tau \rangle = 6$ ps, see Supporting Information). The slow rate explains why the 2D IR does not reveal any clear cross-peak within the investigated time window. Therefore, the two underlying peaks in the amide I cannot be assigned to different solvation structures formed by thermally induced conformers.

Other possible mechanisms to explain the presence of two bands are different dimer- D_2O interactions, intra- and intermolecular hydrogen bonding, aggregation, and the presence of conformers. First, the solvation shell structure in an aqueous dimer solution derived from the MD simulations shows that the carbonyl groups in the dimer have an average of two water molecules in the first solvation shell, which is similar to the monomer (see Supporting Information). This result indicates an analogous first solvation shell structure in the monomer and the dimer. Moreover, the direct interaction of the dimer with water molecules is deduced from the ultrafast dynamics of spectral diffusion (characteristic time of 1.3 ± 0.4 ps, see Table 1), which is very similar to that of the monomer. The strong similarity between the solvation structure and dynamics of the spectral diffusion for the monomer and dimer illustrates the resemblance of amide hydration shell irrespective of the molecular structure. Second, the MD simulations reveal that the dimer does not appear to form appreciable amounts of

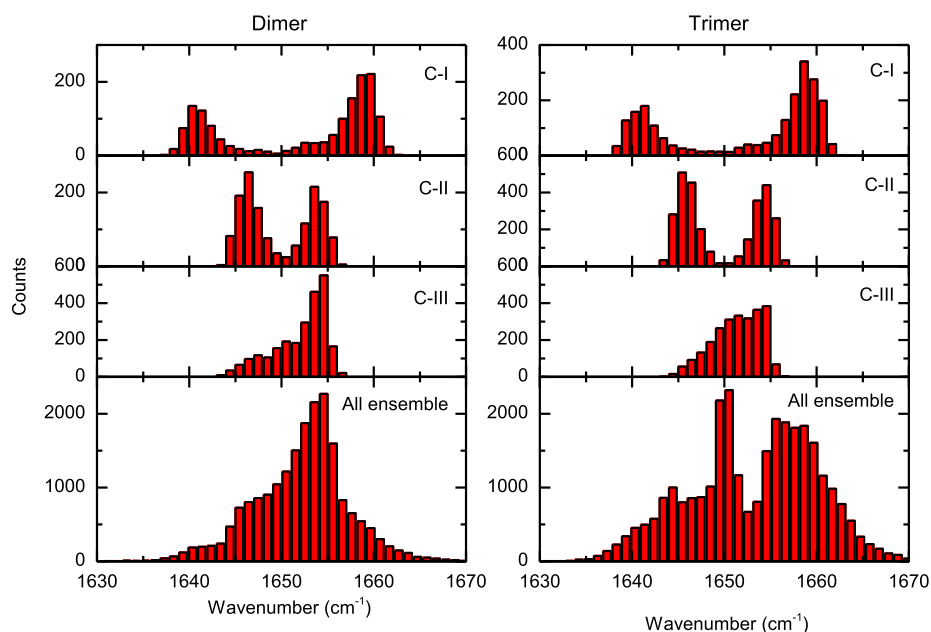


Figure 4. Frequency distributions for the dimer (left panels) and trimer (right panels). In both cases, the top three panels display representative distributions for the C-I, C-II, and C-III conformers, and the bottom panel displays the whole ensemble calculated from MD simulations at 300 K.

intramolecular hydrogen bonds in aqueous solution. Third, concentration-dependent linear IR and MD simulation do not show formation of aggregates (not shown). Thus, the two underlying bands in the linear IR and 2D IR spectra of the dimer cannot be explained by any of the following mechanisms: degree of hydration of the amides, intramolecular and intermolecular hydrogen bonding, aggregation, and solvation structure because of side chain rotation. Hence, the two underlying bands in the amide I band of the dimer arise from dimer conformers. It is important to note that the dimer conformers are observed in the IR spectra because the two amide I transitions of the dimer are vibrationally coupled, which results in a split amide I transitions in the conformers.^{93,94} The presence of conformers with split and coupled amide I transitions is supported by the IR spectra of the dimer in THF (see [Supporting Information](#)), which can only be explained by the presence of conformations that are vibrationally coupled.

The hypothesis that the second transition in the IR spectra of the dimer is caused by the presence of conformers with vibrationally coupled transitions is tested by computing the instantaneous amide I modes using the MD trajectory and the transition dipole coupling (TDC) model.^{60,95} In the TDC model, the vibrational coupling constant between the two amides is determined by the distance and orientation between the two amide groups⁷⁰ and is given by

$$\beta_{ij} = \frac{1}{4\pi\epsilon_0} \left[\frac{\vec{\mu}_i \cdot \vec{\mu}_j}{r_{ij}^3} - 3 \frac{(\vec{r}_{ij} \cdot \vec{\mu}_i)(\vec{r}_{ij} \cdot \vec{\mu}_j)}{r_{ij}^5} \right] \quad (2)$$

where $\vec{\mu}_i$ is the transition dipole of the local modes, \vec{r}_{ij} is the vector connecting the sites i and j . In this case, the histogram of frequencies derived from the computations shows that the amide I band is clearly asymmetric ([Figure 4](#)). Moreover, the asymmetry revealed by the model agrees well with the IR spectrum because the high frequency side has a higher intensity than the low frequency side. Finally, the average weighted frequency is 2.2 cm^{-1} higher for the dimer as

compared to the uncoupled amide I (1650 cm^{-1}) indicating that the observed blue shift in the IR spectrum is caused by the vibrationally coupled nature of the amide I transitions in the dimer.

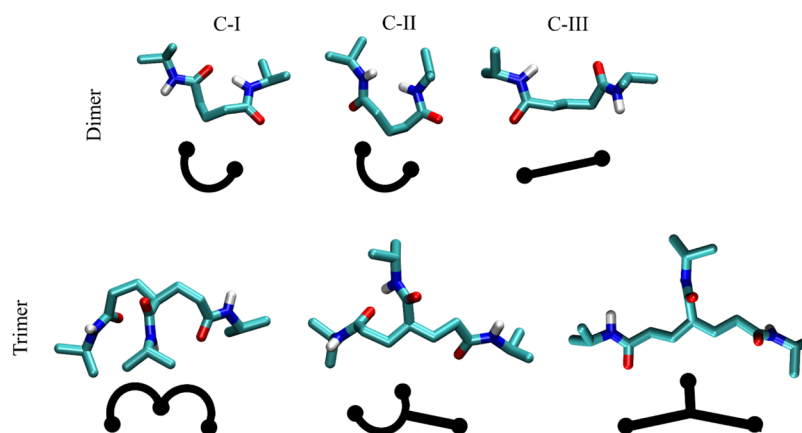
The assignment of the asymmetry to conformation of the dimers is supported by the MD simulation, where these molecular arrangements are observed directly in the distribution of the distance between the two carbonyl carbons. In this case, it is observed that two main conformers with a $\langle r_{C-C} \rangle$ of ~ 3.8 and ~ 4.6 Å that account for $\sim 94\%$ probability exist in the dimer while a third conformer with a $\langle r_{C-C} \rangle$ of ~ 5.1 Å accounts for the rest (probability $\sim 6\%$). Because of the negligible contribution of the latter, the focus of the discussion will be on the conformers with $\langle r_{C-C} \rangle$ smaller than 5.0 Å. The conformation with a $\langle r_{C-C} \rangle \sim 3.8$ Å represents two different amide arrangements with different r_{N-N} and r_{O-O} distances, but the conformer with an $\langle r_{C-C} \rangle \sim 4.6$ Å is almost entirely composed of a single amide arrangement. Thus, the dimer has three most probable conformers: C-I, C-II, and C-III (see [Table 2](#) and [Scheme 2](#)). Notably, the average structures of C-I

Table 2. Amide–Amide Distance Parameters Used to Define the Dimer Conformers

conformers	r_{C-C} (Å)	r_{O-O} (Å)	r_{N-N} (Å)
C-I	3.8	4.7	5.1
C-II	3.8	5.4	4.0
C-III	4.6	5.5	6.0

and C-II show that the main chain alkyl backbone is significantly compact (i.e., close amide side chains),⁹⁶ but C-III has a fairly extended backbone. The histograms of the frequencies computed with the TDC model for C-I, C-II, and C-III are depicted in [Figure 4](#). It is observed that the conformers C-I and C-II have clearly split distribution of frequencies, but not C-III, which is consistent with the extended backbone structure with not so well-defined amide–amide orientation. However, the histogram of frequencies

Scheme 2. Snapshots and Cartoons of Representative Geometries Retrieved from MD Simulation for Dimer (Top) and Trimer (Bottom)^a.



^aC-I (compact), C-II (intermediate), and C-III (open) are shown from left to right. The trimer conformers show some possible combinations compact (C-I, C-I), intermediate (C-I or C-II and C-III), and open (C-III, C-III).

corresponding to the C-III conformer shows a clear spread in frequency and asymmetry in the intensities, which also arise from vibrational coupling.⁷⁰ Therefore, it is reasonable to assign the low and high frequency bands in the linear IR of the aqueous dimer to a split amide I transition as a result of the presence of C-I, C-II, and C-III, all of which have the signatures of vibrational coupling. The observation confirms that the dimer has distinct backbone structures (conformers), each with its distinct IR signature because of the unique spatial arrangement of the two amide groups in these conformers.

To validate the model based on vibrational coupling and conformations as the mechanism for the split amide I band, the temperature effect of dimer in the linear IR is studied experimentally and theoretically. The temperature-dependent linear IR shows a band narrowing and a shift to higher frequencies with temperature (see Supporting Information), which agrees with an increase in the $\langle r_{C-C} \rangle$ of the dimer from ~ 4.6 to ~ 5.1 Å and the narrow shift to higher frequency of its IR histogram derived from the MD simulation at higher temperatures (see Supporting Information). In addition, the modeling of the IR band is further supported by the 2D IR of the dimer in different solvents. In the case of the amide I transitions of the C-I, the two transitions are vibrationally coupled and it would be expected to have a vibrational signature in the 2D IR spectra in the form of a cross-peak at early waiting times.⁷⁰ Even though cross peaks are not clearly observed at any of the measured waiting times because they are buried in homogeneously broadened amide I band in water,⁶³ the 2DIR spectrum of the dimer in THF at $T_w = 0$ ps shows the presence of the cross-peak, which validates the idea that when the amides are sufficiently close, they are vibrationally coupled. Finally, the presence of multiple conformers is supported by the offset observed in the modeling of the spectral diffusion (Table 1), which significantly increases from the monomer to the dimer. The large increase in the offset is likely to be caused by the presence of many conformers (inhomogeneous distributions) within the amide I band that do not exchange within the observation window because of their slow interconversions.⁹⁰ It is important to note that the offset, observed in the FFCF and assigned to the presence of overlapping amide I transitions, could also arise from a long-lived dynamical component. However, the offset is not

assigned to such slow dynamic processes because the hydrogen bond dynamics between the amide and water derived from the MD simulation did not show any slow component (see Supporting Information).

Trimer. The linear IR and 2DIR spectra of the trimer present a broad and asymmetric IR band, and the two underlying bands appear to be located at 1610 and 1625 cm^{-1} . In addition, the dynamics of the spectral diffusion evaluated from the slope in 2D IR spectra using eq 1 shows a decay time constant of 0.6 ± 0.2 ps and an offset of ~ 0.49 , which within the experimental error is similar to that observed for the monomer and the dimer. Moreover, the analysis of the MD trajectory shows that the trimer carbonyl groups have an average of two water molecules in their first solvation shell (see Supporting Information), indicating the trimer has a comparable first solvation shell structure to both the monomer and the dimer. Additionally, no significant intramolecular and intermolecular hydrogen bond formations are observed in the MD simulation. Thus, the resemblance of the experimental and theoretical molecular parameters between the trimer and dimer allows us to deduce that the molecular mechanism behind the shape of amide I band is likely to be the same in these two oligomers. This is also supported by the frequency distribution of the trimer computed from the MD using a TDC model. In this case, the histogram shows an asymmetric distribution of frequencies (Figure 4) in agreement with the experimental linear and nonlinear spectra (Figures 1 and 2). Moreover, as previously deduced for the dimer, it is likely that the asymmetry in the amide I band is caused by the effect of the vibrational coupling into the transition dipole magnitude and frequency split from distinct arrangements of amide side chains or, equivalently, distinct backbone conformers.

Analysis of the distance distribution between each of the terminal amide units (T_{A1} and T_{A2}) and the central amide (C_A) reveals the trimer has very similar backbone conformer distribution as the dimer. In each conformer, the two neighboring amides ($T_{A1}-C_A$ and $T_{A2}-C_A$) have mainly two carbonyl carbon–carbon distance distributions with $\langle r_{C-C} \rangle$ of ~ 3.8 and ~ 4.5 Å. In addition, as in the dimer, the conformer with $\langle r_{C-C} \rangle$ of ~ 3.8 Å represents two distinct conformers with different r_{N-N} and r_{O-O} distances, while the conformer with a $\langle r_{C-C} \rangle \sim 4.6$ Å is almost entirely composed of a single amide

arrangement. The carbonyl carbon distance distribution between the two terminal amides (T_{A1} and T_{A2}) shows two conformations with $\langle r_{C-C} \rangle$ of ~ 5.7 and ~ 6.9 Å. Overall, the geometry of the trimer is defined by the co-existing combination of the three conformers of C-I, C-II, and C-III in each of the side (Scheme 2). In other words, the trimer has conformations where it is compact when the central and side amides (T_{A1-C_A} and T_{A2-C_A}) have C-I and C-II conformations, is open when both side amides have C-III conformation with the central amide, and is in an intermediate state when one side is in either C-I or C-II and the other adopts a C-III conformation.

The histogram of frequencies and coupling for the C-I, C-II, and C-III conformers of the trimer was computed from the MD simulation. The frequency distribution for C-I, C-II, and C-III conformers of a representative T_A-C_A is shown in Figure 4. Similar to the dimer, the conformers C-I and C-II have split frequency distributions. Thus, it can be deduced that the presence of these conformers with specific amide I band signatures gives rise to an asymmetric distribution of frequencies in the whole ensemble of the trimer. Moreover, the frequency distribution histogram of the whole ensemble semiquantitatively reproduces the shape of the trimer amide I band. In particular, it reproduces well the higher intensity of the high frequency part of the band. In addition, the trimer has a blueshift in the average weighted frequency of its amide I band (3.2 cm^{-1} higher than the uncoupled amide and 1.0 cm^{-1} higher than the dimer), which corroborates our previous indication that the coupled nature of the amide I band is responsible for the direct relation between shift of the amide I transition and the number of units in the oligomers. Overall, the results demonstrate that the trimer does not have a random structure. Rather, it has distinct backbone structures with distinct IR signatures, which are mainly defined by the vibrational coupling between nearest-neighboring amides as in the dimer. Moreover, it is clear that the presence of the third monomeric unit does not modify the interaction between neighboring amides. Therefore, it is reasonable to assign the observed split amide I band to the presence of distinct backbone conformations in the trimer, as previously deduced for the dimer.

Polymer (PNIPAM). As in the oligomers, the linear and nonlinear IR spectra of PNIPAM in D_2O show two transitions within the amide I band. However, they too show the presence of a third transition in its high frequency side, which is easier to observe in the 2D IR spectra. Modeling of the amide I of the polymer reveals that these three bands are located at 1612, 1628, and 1647 cm^{-1} . It is important to note that the Voigt profile model of the amide I might not accurately describe the lineshape of these peaks, but it is the most reasonable modeling to obtain spectral parameters. Previous FTIR studies on amide I band of PNIPAM in aqueous solution did not report the high frequency band below the LCST, but mentioned its growth above this temperature.^{25,97} However, this band was reported in a UV resonance Raman study though the frequency position of the band was slightly different because the experiment was performed in H_2O .²⁷ Interestingly, the higher frequency band (1647 cm^{-1}) shows no appreciable evolution in the spectral diffusion and so is ascribed to the dehydrated amide side chains of the polymer, probably arising from amide sites buried in the random coil and not interacting with water. This assignment is in agreement with previous reports.^{25,26,41,48,97}

The two intense bands located at 1612 and 1628 cm^{-1} are likely to be caused by different backbone conformations similar to the dimer and trimer. This assignment is supported by the linear and nonlinear IR spectra of PNIPAM in THF (see Supporting Information), which not only displays two split transitions but also a cross-peak between them at $T_w = 0$ fs. In addition, the slope of spectral diffusion (Figure 3) shows a nonexponential behavior, which is attributed to the excitonic nature of the vibrational manifold of the polymer arising from the vibrational coupling among different amides of the polymer. A similar behavior in the spectral diffusion was observed in the hydrophobic collapse of *N*-methylacetamide in water, which was also explained in terms of vibrational coupling.⁹⁸

Because the addition of a unit to the dimer does not affect the backbone conformation of the trimer, it is reasonable to expect that the addition of multiple monomeric units will result in the same structure among neighboring amide groups. In other words, it is inferred from the lack of changes seen by investigating the dimer to the trimer that the adjacent amide side chains of PNIPAM will adopt the same conformations as observed in the two oligomers. Hence, it is inferred that the same backbone conformations (C-I, C-II, and C-III) exist in PNIPAM and the two low frequency bands of the polymer (~ 1612 and 1628 cm^{-1}) correspond to the split amide I band arising from vibrational coupling between neighboring amides.

To test the model of vibrational coupling as the source of the amide I split, the changes in the amide I band of the polymer with temperature below the LCST were used as a prediction of the change in the polymer structure. In the polymer solutions, the amide I gets broader as temperature increases as seen in its fwhm (Figure 5). While the variation in

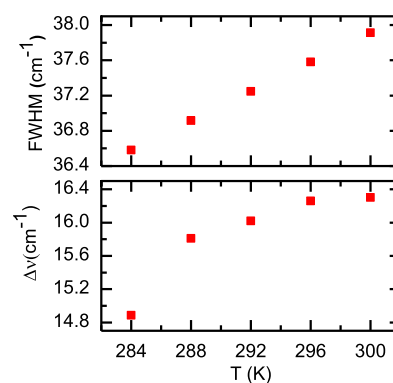


Figure 5. PNIPAM amide I band parameters as function of temperature. The top panel shows fwhm, and the bottom panel shows the difference in the peak position frequency for the two major underlying peaks (bottom panel).

the fwhm could be caused by the change in the intensity of one or both of the two underlying amide I bands, the frequency separation between the two main bands, determined by fitting with two Voigt profiles, also increases with temperature (see Figure 5 and Supporting Information). This suggests that the change in fwhm is directly affected by the change in the frequency separation between amide I bands. In the context of our model, the observed changes in the amide I band with temperature are explained by changes in the backbone conformation arising from different vibrational coupling between neighboring amide side chains. Thus, an increase in the fwhm or frequency separation denotes an increase in the

splitting of the amide I band because of a stronger coupling among amide side chains and corresponds to a larger population of C-I and C-II conformers (Figure 4). Because of the specific backbone conformation of C-I and C-II, the presence of larger concentration of these two conformers should result in a more compact polymer. This model prediction is exactly what is observed experimentally because a previous report showed that the radius of gyration of the polymer decreases with temperature below the LCST.⁴⁰ Thus, the presented model can explain the observed change in the amide I band with temperature below the LCST. Overall, the result strongly suggests that the PNIPAM amide I band is dominated by vibrational coupling which are manifested as split vibrational transitions within the amide I band. Below the LCST, this changes directly reflect the changes in the backbone conformation of the polymer.

SUMMARY

In this study, linear and nonlinear IR spectroscopies in combination with MD simulations were used to investigate the molecular structure of aqueous solutions of poly(*N*-isopropylacrylamide) (PNIPAM) and its monomer, dimer, and trimer. In all the samples, the amide I band was found to have more than one transition. Computational modeling and the 2D IR spectra showed the amide I band has two transitions in the monomer and the oligomers, while in PNIPAM, three transitions were observed. In the monomer, temperature dependence and enthalpy changes revealed the transitions were not from amide units with different hydrogen-bonded states, but from rotational conformers with different solvation structures. In the oligomers, on the other hand, experimental and theoretical structural analyses showed that three distinct backbone conformers exist. Two of these conformers have amide groups with a closed proximity ($\langle r_{C-C} \rangle \sim 3.8$ Å) or, equivalently, a compact and closed backbone, while the third one has amides far apart by $\langle r_{C-C} \rangle \sim 4.6$ Å and the backbone is relatively extended. Instantaneous frequency modeling by TDC showed that the closed conformers have significant vibrational coupling. In the trimer, it was found that its geometry could be represented by a co-existing combination of the conformers observed in dimer because the third amide unit did not appear to change the conformation of neighboring amides. Interestingly, the theoretical modeling of the amide I band of the dimer and trimer semiquantitatively reproduces the experimental result, indicating that the amide I band has a split IR transition from vibrational coupling among amide side chains. It is, therefore, implied that the same conformers exist in the polymer and that the two lower frequency bands originate from the same vibrational coupling mechanism. The proposed mechanism is further supported by other experimental observations. For example, it successfully describes the variation of the amide I band of PNIPAM with temperature in terms of the changes in the proximity among amide side chains (polymer structure) below the phase transition temperature. Finally, the deduced molecular model strongly suggests that PNIPAM does not have a completely random backbone because it is defined by distinct backbone conformations in between two neighboring amides.

ASSOCIATED CONTENT

Supporting Information

The Supporting Information is available free of charge at <https://pubs.acs.org/doi/10.1021/acs.jpcb.0c08424>.

Synthesis of monomer and oligomers. Linear FTIR fitting parameters for monomer, oligomers, and PNIPAM in D₂O, van't Hoff plot fitting parameters and calculated enthalpy and entropy for monomer, autocorrelation parameters for dihedral angle decay for monomer and dimer, fitting parameters for linear FTIR of monomer, dimer, and PNIPAM in THF, fitting parameters for the linear FTIR of PNIPAM temperature dependence, van't Hoff plot of monomer in D₂O, dynamics of the dihedral angle of the monomer and dimer, radial distribution function for the monomer, dimer, and trimer, autocorrelation dynamics for the hydrogen bonds between the carbonyl group of the amide and water, dimer temperature dependence linear IR, MD simulation frequency distribution for dimer at 350 K, linear IR and 2D IR spectra of the monomer, dimer, and PNIPAM in THF, and temperature dependence spectra of PNIPAM (PDF)

AUTHOR INFORMATION

Corresponding Author

Daniel G. Kuroda – Department of Chemistry, Louisiana State University, Baton Rouge, Louisiana 70803, United States; orcid.org/0000-0002-4752-7024; Phone: (+1) 225-578-1780; Email: dkuroda@lsu.edu

Authors

Habtom B. Gobeze – Department of Chemistry, Louisiana State University, Baton Rouge, Louisiana 70803, United States

Jianbo Ma – Department of Chemistry, Louisiana State University, Baton Rouge, Louisiana 70803, United States

Fedra M. Leonik – Department of Chemistry, Louisiana State University, Baton Rouge, Louisiana 70803, United States

Complete contact information is available at:

<https://pubs.acs.org/doi/10.1021/acs.jpcb.0c08424>

Notes

The authors declare no competing financial interest.

ACKNOWLEDGMENTS

The authors acknowledge financial support from the Chemistry Department. The authors also acknowledge the High Performance Computing Center at Louisiana State University and the Louisiana Optical Network Initiative (LONI) for computer time.

REFERENCES

- (1) Hoffman, A. S. Stimuli-responsive polymers: Biomedical applications and challenges for clinical translation. *Adv. Drug Delivery Rev.* **2013**, *65*, 10–16.
- (2) Galaev, I.; Mattiasson, B. 'Smart' polymers and what they could do in biotechnology and medicine. *Trends Biotechnol.* **1999**, *17*, 335–340.
- (3) Pelton, R. Temperature-sensitive aqueous microgels. *Adv. Colloid Interface Sci.* **2000**, *85*, 1–33.
- (4) Abulateefeh, S. R.; Spain, S. G.; Aylott, J. W.; Chan, W. C.; Garnett, M. C.; Alexander, C. Thermoresponsive polymer colloids for drug delivery and cancer therapy. *Macromol. Biosci.* **2011**, *11*, 1722–1734.
- (5) Bergueiro, J.; Calderón, M. Thermoresponsive nanodevices in biomedical applications. *Macromol. Biosci.* **2015**, *15*, 183–199.

- (6) Kim, Y.-J.; Matsunaga, Y. T. Thermo-responsive polymers and their application as smart biomaterials. *J. Mater. Chem. B* **2017**, *5*, 4307–4321.
- (7) Klouda, L.; Mikos, A. G. Thermoresponsive hydrogels in biomedical applications. *Eur. J. Pharm. Biopharm.* **2008**, *68*, 34–45.
- (8) Hruby, M.; Kucka, J.; Lebeda, O.; Mackova, H.; Babic, M.; Konak, C.; Studenovský, M.; Sikora, A.; Kozempel, J.; Ulbrich, K. New bioerodable thermoresponsive polymers for possible radiotherapeutic applications. *J. Controlled Release* **2007**, *119*, 25–33.
- (9) Ward, M. A.; Georgiou, T. K. Thermoresponsive polymers for biomedical applications. *Polymers* **2011**, *3*, 1215–1242.
- (10) Gandhi, A.; Paul, A.; Sen, S. O.; Sen, K. K. Studies on thermoresponsive polymers: Phase behaviour, drug delivery and biomedical applications. *Asian J. Pharm. Sci.* **2015**, *10*, 99–107.
- (11) Khutoryanskiy, V. V.; Georgiou, T. K. *Temperature-responsive polymers: Chemistry, properties and applications*; Wiley-Blackwell, 2018.
- (12) Heskins, M.; Guillet, J. E. Solution properties of poly(n-isopropylacrylamide). *J. Macromol. Sci., Part A: Pure Appl. Chem.* **1968**, *2*, 1441–1455.
- (13) Shim, H.; McCullough, E. A.; Jones, B. W. Using phase change materials in clothing. *Text. Res. J.* **2001**, *71*, 495–502.
- (14) Liu, L.; Sheardown, H. Glucose permeable poly (dimethyl siloxane) poly (n-isopropyl acrylamide) interpenetrating networks as ophthalmic biomaterials. *Biomaterials* **2005**, *26*, 233–244.
- (15) Li, W.; Huang, L.; Ying, X.; Jian, Y.; Hong, Y.; Hu, F.; Du, Y. Antitumor drug delivery modulated by a polymeric micelle with an upper critical solution temperature. *Angew. Chem., Int. Ed. Engl.* **2015**, *54*, 3126–3131.
- (16) Kikuchi, A.; Okano, T. Intelligent thermoresponsive polymeric stationary phases for aqueous chromatography of biological compounds. *Prog. Polym. Sci.* **2002**, *27*, 1165–1193.
- (17) Lanzalaco, S.; Armelin, E. Poly(n-isopropylacrylamide) and copolymers: A review on recent progresses in biomedical applications. *Gels-Basel* **2017**, *3*, 36.
- (18) Terada, T.; Inaba, T.; Kitano, H.; Maeda, Y.; Tsukida, N. Raman-spectroscopic study on water in aqueous-solutions of temperature-responsive polymers - poly(n-isopropylacrylamide) and poly[n-(3-ethoxypropyl)acrylamide]. *Macromol. Chem. Phys.* **1994**, *195*, 3261–3270.
- (19) Maeda, Y.; Yamamoto, H.; Ikeda, I. Phase separation of aqueous solutions of poly (n-isopropylacrylamide) investigated by confocal raman microscopy. *Macromolecules* **2003**, *36*, 5055–5057.
- (20) Wang, X.; Qiu, X.; Wu, C. Comparison of the coil-to-globule and the globule-to-coil transitions of a single poly(n-isopropylacrylamide) homopolymer chain in water. *Macromolecules* **1998**, *31*, 2972–2976.
- (21) Wu, C.; Wang, X. Globule-to-coil transition of a single homopolymer chain in solution. *Phys. Rev. Lett.* **1998**, *80*, 4092–4094.
- (22) Wu, C.; Zhou, S. Laser-light scattering study of the phase-transition of poly(n-isopropylacrylamide) in water .1. Single-chain. *Macromolecules* **1995**, *28*, 8381–8387.
- (23) Wu, C.; Zhou, S. Thermodynamically stable globule state of a single poly(n-isopropylacrylamide) chain in water. *Macromolecules* **1995**, *28*, 5388–5390.
- (24) Kubota, K.; Fujishige, S.; Ando, I. Single-chain transition of poly(n-isopropylacrylamide) in water. *J. Phys. Chem.* **1990**, *94*, 5154–5158.
- (25) Maeda, Y.; Higuchi, T.; Ikeda, I. Change in hydration state during the coil-globule transition of aqueous solutions of poly(n-isopropylacrylamide) as evidenced by ftir spectroscopy. *Langmuir* **2000**, *16*, 7503–7509.
- (26) Sun, B.; Lin, Y.; Wu, P.; Siesler, H. W. A ftir and 2d-ir spectroscopic study on the microdynamics phase separation mechanism of the poly(n-isopropylacrylamide) aqueous solution. *Macromolecules* **2008**, *41*, 1512–1520.
- (27) Ahmed, Z.; Gooding, E. A.; Pimenov, K. V.; Wang, L.; Asher, S. A. Uv resonance raman determination of molecular mechanism of poly(n-isopropylacrylamide) volume phase transition. *J. Phys. Chem. B* **2009**, *113*, 4248–4256.
- (28) Fujishige, S.; Kubota, K.; Ando, I. Phase-transition of aqueous-solutions of poly(n-isopropylacrylamide) and poly(n-isopropylmethacrylamide). *J. Phys. Chem.* **1989**, *93*, 3311–3313.
- (29) Tiktopulo, E. I.; Bychkova, V. E.; Ricka, J.; Ptitsyn, O. B. Cooperativity of the coil-globule transition in a homopolymer - microcalorimetric study of poly(n-isopropylacrylamide). *Macromolecules* **1994**, *27*, 2879–2882.
- (30) Feil, H.; Bae, Y. H.; Feijen, J.; Kim, S. W. Effect of comonomer hydrophilicity and ionization on the lower critical solution temperature of n-isopropylacrylamide copolymers. *Macromolecules* **1993**, *26*, 2496–2500.
- (31) Inomata, H.; Goto, S.; Otake, K.; Saito, S. Effect of additives on phase-transition of n-isopropylacrylamide gels. *Langmuir* **1992**, *8*, 687–690.
- (32) Schild, H. G.; Tirrell, D. A. Microcalorimetric detection of lower critical solution temperatures in aqueous polymer-solutions. *J. Phys. Chem.* **1990**, *94*, 4352–4356.
- (33) Walter, R.; Rička, J.; Quillet, C.; Nyffenegger, R.; Binkert, T. Coil-globule transition of poly(n-isopropylacrylamide): A study of polymer-surfactant association. *Macromolecules* **1996**, *29*, 4019–4028.
- (34) Winnik, F. M. Fluorescence studies of aqueous-solutions of poly(n-isopropylacrylamide) below and above their lcst. *Macromolecules* **1990**, *23*, 233–242.
- (35) Qiu, X.; Kwan, C. M. S.; Wu, C. Laser light scattering study of the formation and structure of poly(n-isopropylacrylamide-co-acrylic acid) nanoparticles. *Macromolecules* **1997**, *30*, 6090–6094.
- (36) Meewes, M.; Ricka, J.; De Silva, M.; Nyffenegger, R.; Binkert, T. Coil globule transition of poly(n-isopropylacrylamide) - a study of surfactant effects by light-scattering. *Macromolecules* **1991**, *24*, 5811–5816.
- (37) Chen, J.; Gong, X.; Yang, H.; Yao, Y.; Xu, M.; Chen, Q.; Cheng, R. Nmr study on the effects of sodium n-dodecyl sulfate on the coil-to-globule transition of poly(n-isopropylacrylamide) in aqueous solutions. *Macromolecules* **2011**, *44*, 6227–6231.
- (38) Burba, C. M.; Carter, S. M.; Meyer, K. J.; Rice, C. V. Salt effects on poly(n-isopropylacrylamide) phase transition thermodynamics from nmr spectroscopy. *J. Phys. Chem. B* **2008**, *112*, 10399–10404.
- (39) Dybal, J.; Trchová, M.; Schmidt, P. The role of water in structural changes of poly(n-isopropylacrylamide) and poly(n-isopropylmethacrylamide) studied by ftir, raman spectroscopy and quantum chemical calculations. *Vib. Spectrosc.* **2009**, *51*, 44–51.
- (40) Cheng, H.; Shen, L.; Wu, C. Lls and ftir studies on the hysteresis in association and dissociation of poly(n-isopropylacrylamide) chains in water. *Macromolecules* **2006**, *39*, 2325–2329.
- (41) Meersman, F.; Wang, J.; Wu, Y.; Heremans, K. Pressure effect on the hydration properties of poly(n-isopropylacrylamide) in aqueous solution studied by ftir spectroscopy. *Macromolecules* **2005**, *38*, 8923–8928.
- (42) Maeda, Y.; Higuchi, T.; Ikeda, I. Ftir spectroscopic and calorimetric studies of the phase transitions of n-isopropylacrylamide copolymers in water. *Langmuir* **2001**, *17*, 7535–7539.
- (43) Lai, H.; Wu, P. A infrared spectroscopic study on the mechanism of temperature-induced phase transition of concentrated aqueous solutions of poly(n-isopropylacrylamide) and n-isopropylpropionamide. *Polymer* **2010**, *51*, 1404–1412.
- (44) Maeda, Y.; Nakamura, T.; Ikeda, I. Changes in the hydration states of poly(n-alkylacrylamide)s during their phase transitions in water observed by ftir spectroscopy. *Macromolecules* **2001**, *34*, 1391–1399.
- (45) Tu, C.-W.; Kuo, S.-W. Using ftir spectroscopy to study the phase transitions of poly(n-isopropylacrylamide) in tetrahydrofuran-d(8)/d2o. *J. Polym. Res.* **2014**, *21*, 476.
- (46) Park, Y.; Hashimoto, C.; Ozaki, Y.; Jung, Y. M. Understanding the phase transition of linear poly(n-isopropylacrylamide) gel under the heating and cooling processes. *J. Mol. Struct.* **2016**, *1124*, 144–150.
- (47) Juurinen, I.; Galambosi, S.; Anghelescu-Hakala, A. G.; Koskelo, J.; Honkimäki, V.; Hämäläinen, K.; Huotari, S.; Hakala, M. Molecular-

level changes of aqueous poly(*n*-isopropylacrylamide) in phase transition. *J. Phys. Chem. B* **2014**, *118*, 5518–5523.

(48) Futscher, M. H.; Philipp, M.; Müller-Buschbaum, P.; Schulte, A. The role of backbone hydration of poly(*n*-isopropyl acrylamide) across the volume phase transition compared to its monomer. *Sci. Rep.* **2017**, *7*, 17012.

(49) Ono, Y.; Shikata, T. Contrary hydration behavior of *n*-isopropylacrylamide to its polymer, p(*n*ipam), with a lower critical solution temperature. *J. Phys. Chem. B* **2007**, *111*, 1511–1513.

(50) Ono, Y.; Shikata, T. Hydration and dynamic behavior of poly(*n*-isopropylacrylamide)s in aqueous solution: A sharp phase transition at the lower critical solution temperature. *J. Am. Chem. Soc.* **2006**, *128*, 10030–10031.

(51) Deshmukh, S. A.; Sankaranarayanan, S. K. R. S.; Suthar, K.; Mancini, D. C. Role of solvation dynamics and local ordering of water in inducing conformational transitions in poly(*n*-isopropylacrylamide) oligomers through the lcst. *J. Phys. Chem. B* **2012**, *116*, 2651–2663.

(52) Kang, Y.; Joo, H.; Kim, J. S. Collapse-swelling transitions of a thermoresponsive, single poly(*n*-isopropylacrylamide) chain in water. *J. Phys. Chem. B* **2016**, *120*, 13184–13192.

(53) Tucker, A. K.; Stevens, M. J. Study of the polymer length dependence of the single chain transition temperature in syndiotactic poly(*n*-isopropylacrylamide) oligomers in water. *Macromolecules* **2012**, *45*, 6697–6703.

(54) Podewitz, M.; Wang, Y.; Quoika, P. K.; Loeffler, J. R.; Schauperl, M.; Liedl, K. R. Coil-globule transition thermodynamics of poly(*n*-isopropylacrylamide). *J. Phys. Chem. B* **2019**, *123*, 8838–8847.

(55) Torii, H.; Tasumi, M. Model-calculations on the amide-i infrared bands of globular-proteins. *J. Chem. Phys.* **1992**, *96*, 3379–3387.

(56) Krimm, S.; Bandekar, J. Vibrational spectroscopy and conformation of peptides, polypeptides, and proteins. *Adv. Protein Chem.* **1986**, *38*, 181–364.

(57) Torii, H.; Tasumi, M. Ab initio molecular orbital study of the amide i vibrational interactions between the peptide groups in di- and tripeptides and considerations on the conformation of the extended helix. *J. Raman Spectrosc.* **1998**, *29*, 81–86.

(58) Measey, T.; Schweitzer-Stenner, R. Simulation of amide i' band profiles of trans polyproline based on an excitonic coupling model. *Chem. Phys. Lett.* **2005**, *408*, 123–127.

(59) Kim, Y. S.; Hochstrasser, R. M. Applications of 2d ir spectroscopy to peptides, proteins, and hydrogen-bond dynamics. *J. Phys. Chem. B* **2009**, *113*, 8231–8251.

(60) Ganim, Z.; Chung, H. S.; Smith, A. W.; Deflores, L. P.; Jones, K. C.; Tokmakoff, A. Amide i two-dimensional infrared spectroscopy of proteins. *Acc. Chem. Res.* **2008**, *41*, 432–441.

(61) Strasfeld, D. B.; Ling, Y. L.; Gupta, R.; Raleigh, D. P.; Zanni, M. T. Strategies for extracting structural information from 2d ir spectroscopy of amyloid: Application to islet amyloid polypeptide. *J. Phys. Chem. B* **2009**, *113*, 15679–15691.

(62) Finkelstein, I. J.; Zheng, J.; Ishikawa, H.; Kim, S.; Kwak, K.; Fayer, M. D. Probing dynamics of complex molecular systems with ultrafast 2d ir vibrational echo spectroscopy. *Phys. Chem. Chem. Phys.* **2007**, *9*, 1533–1549.

(63) Rubtsov, I. V.; Wang, J.; Hochstrasser, R. M. Dual frequency 2d-ir of peptide amide-a and amide-i modes. *J. Chem. Phys.* **2003**, *118*, 7733–7736.

(64) Ma, J.; Xuan, S.; Guerin, A. C.; Yu, T.; Zhang, D.; Kuroda, D. G. Unusual molecular mechanism behind the thermal response of polypeptoids in aqueous solutions. *Phys. Chem. Chem. Phys.* **2017**, *19*, 10878–10888.

(65) Hamm, P.; Lim, M.; Hochstrasser, R. M. Structure of the amide i band of peptides measured by femtosecond nonlinear-infrared spectroscopy. *J. Phys. Chem. B* **1998**, *102*, 6123–6138.

(66) Cui, Y.; Rushing, J. C.; Seifert, S.; Bedford, N. M.; Kuroda, D. G. Molecularly heterogeneous structure of a nonionic deep eutectic solvent composed of *n*-methylacetamide and lauric acid. *J. Phys. Chem. B* **2019**, *123*, 3984–3993.

(67) Wang, J.; Chen, J.; Hochstrasser, R. M. Local structure of beta-hairpin isotopomers by ftir, 2d ir, and ab initio theory. *J. Phys. Chem. B* **2006**, *110*, 7545–7555.

(68) Ganim, Z.; Tokmakoff, A. Spectral signatures of heterogeneous protein ensembles revealed by md simulations of 2dir spectra. *Biophys. J.* **2006**, *91*, 2636–2646.

(69) Smith, A. W.; Tokmakoff, A. Probing local structural events in β -hairpin unfolding with transient nonlinear infrared spectroscopy. *Angew. Chem., Int. Ed. Engl.* **2007**, *46*, 7984–7987.

(70) Hamm, P.; Zanni, M. *Concepts and methods of 2d infrared spectroscopy*; Cambridge University Press: Cambridge, 2011.

(71) Ghosh, A.; Ostrander, J. S.; Zanni, M. T. Watching proteins wiggle: Mapping structures with two-dimensional infrared spectroscopy. *Chem. Rev. (Washington, DC, U.S.)* **2017**, *117*, 10726–10759.

(72) Ishikawa, H.; Kwak, K.; Chung, J. K.; Kim, S.; Fayer, M. D. Direct observation of fast protein conformational switching. *Proc. Natl. Acad. Sci. U.S.A.* **2008**, *105*, 8619–8624.

(73) Zheng, J.; Kwak, K. W.; Xie, J.; Fayer, M. D. Ultrafast carbon-carbon single-bond rotational isomerization in room-temperature solution. *Science (Washington, DC, U.S.)* **2006**, *313*, 1951–1955.

(74) Kuroda, D. G.; Hochstrasser, R. M. Two-dimensional infrared spectral signature and hydration of the oxalate dianion. *J. Chem. Phys.* **2011**, *135*, 204502.

(75) Fulfer, K. D.; Kuroda, D. G. Solvation structure and dynamics of the lithium ion in organic carbonate-based electrolytes: A time-dependent infrared spectroscopy study. *J. Phys. Chem. C* **2016**, *120*, 24011–24022.

(76) Kim, Y. S.; Wang, J.; Hochstrasser, R. M. Two-dimensional infrared spectroscopy of the alanine dipeptide in aqueous solution. *J. Phys. Chem. B* **2005**, *109*, 7511–7521.

(77) Plimpton, S. *Fast parallel algorithms for short-range molecular dynamics*; Sandia National Labs.: Albuquerque, NM (United States), 1993.

(78) Martínez, L.; Andrade, R.; Birgin, E. G.; Martínez, J. M. Packmol: A package for building initial configurations for molecular dynamics simulations. *J. Comput. Chem.* **2009**, *30*, 2157–2164.

(79) Jorgensen, W. L.; Maxwell, D. S.; Tirado-Rives, J. Development and testing of the opls all-atom force field on conformational energetics and properties of organic liquids. *J. Am. Chem. Soc.* **1996**, *118*, 11225–11236.

(80) Kaminski, G. A.; Friesner, R. A.; Tirado-Rives, J.; Jorgensen, W. L. Evaluation and reparametrization of the opls-aa force field for proteins via comparison with accurate quantum chemical calculations on peptides. *J. Phys. Chem. B* **2001**, *105*, 6474–6487.

(81) Darden, T.; York, D.; Pedersen, L. Particle mesh ewald - an nLog(n) method for ewald sums in large systems. *J. Chem. Phys.* **1993**, *98*, 10089–10092.

(82) Guerin, A. C.; Riley, K.; Rupnik, K.; Kuroda, D. G. Determining the energetics of the hydrogen bond through ftir: A hands-on physical chemistry lab experiment. *J. Chem. Educ.* **2016**, *93*, 1124–1129.

(83) Buck, M.; Karplus, M. Hydrogen bond energetics: A simulation and statistical analysis of *n*-methyl acetamide (nma), water, and human lysozyme. *J. Phys. Chem. B* **2001**, *105*, 11000–11015.

(84) MacKerell, A. D.; Karplus, M. Importance of attractive van der waals contribution in empirical energy function models for the heat of vaporization of polar liquids. *J. Phys. Chem.* **1991**, *95*, 10559–10560.

(85) Cahoon, J. F.; Sawyer, K. R.; Schlegel, J. P.; Harris, C. B. Determining transition-state geometries in liquids using 2d-ir. *Science (Washington, DC, U.S.)* **2008**, *319*, 1820–1823.

(86) Galle Kankanamge, S. R.; Ma, J.; Mackin, R. T.; Leonik, F. M.; Taylor, C. M.; Rubtsov, I. V.; Kuroda, D. G. Probing and proving the presence of the elusive c–h···o hydrogen bond in liquid solutions at room temperature. *Angew. Chem., Int. Ed. Engl.* **2020**, *59*, 17012–17017.

(87) Ham, S.; Kim, J.-H.; Lee, H.; Cho, M. Correlation between electronic and molecular structure distortions and vibrational properties. ii. Amide i modes of nma-nd(2)o complexes. *J. Chem. Phys.* **2003**, *118*, 3491–3498.

- (88) Kwac, K.; Cho, M. Molecular dynamics simulation study of n-methylacetamide in water. II. Two-dimensional infrared pump-probe spectra. *J. Chem. Phys.* **2003**, *119*, 2256–2263.
- (89) DeCamp, M. F.; DeFlores, L.; McCracken, J. M.; Tokmakoff, A.; Kwac, K.; Cho, M. Amide I vibrational dynamics of n-methylacetamide in polar solvents: The role of electrostatic interactions. *J. Phys. Chem. B* **2005**, *109*, 11016–11026.
- (90) Kuroda, D. G.; Vorobyev, D. Y.; Hochstrasser, R. M., Ultrafast relaxation and 2d ir of the aqueous trifluorocarboxylate ion. *J. Chem. Phys.* **2010**, *132* (). DOI: 10.1063/1.3285265
- (91) Ghosh, A.; Hochstrasser, R. M. A peptide's perspective of water dynamics. *Chem. Phys.* **2011**, *390*, 1–13.
- (92) Kuo, C.-H.; Hochstrasser, R. M. Two dimensional infrared spectroscopy and relaxation of aqueous cyanide. *Chem. Phys.* **2007**, *341*, 21–28.
- (93) Woutersen, S.; Hamm, P. Isotope-edited two-dimensional vibrational spectroscopy of trialanine in aqueous solution. *J. Chem. Phys.* **2001**, *114*, 2727–2737.
- (94) Mu, Y.; Stock, G. Conformational dynamics of trialanine in water: A molecular dynamics study. *J. Phys. Chem. B* **2002**, *106*, 5294–5301.
- (95) Cheam, T. C.; Krimm, S. Transition dipole interaction in polypeptides - abinitio calculation of transition dipole parameters. *Chem. Phys. Lett.* **1984**, *107*, 613–616.
- (96) Gnanakaran, S.; Hochstrasser, R. M.; Garcia, A. E. Nature of structural inhomogeneities on folding a helix and their influence on spectral measurements. *Proc. Natl. Acad. Sci. U.S.A.* **2004**, *101*, 9229–9234.
- (97) Geukens, B.; Meersman, F.; Nies, E. Phase behavior of n-(isopropyl)propionamide in aqueous solution and changes in hydration observed by ftr spectroscopy. *J. Phys. Chem. B* **2008**, *112*, 4474–4477.
- (98) Salamatova, E.; Cunha, A. V.; Bloem, R.; Roeters, S. J.; Woutersen, S.; Jansen, T. L. C.; Pshenichnikov, M. S. Hydrophobic collapse in n-methylacetamide water mixtures. *J. Phys. Chem. A* **2018**, *122*, 2468–2478.